Empirical Relationships Between Ground Motion Intensities and JMA Seismic Intensity Scale

Authors

Patrick W. Ball[1,*] Toby Sansom[1]

Affiliations

[1] Inigo Insurance Ltd, 25 Fenchurch Avenue, London, United Kingdom, EC3M 5AD

Correspondence

[*] patrick.ball@inigoinsurance.com

June 5, 2026

Empirical Relationships Between Ground Motion Intensities and JMA Seismic Intensity Scale

Non-peer-reviewed preprint submitted to EarthArXiv, compiled June 5, 2026

Patrick W. Ball[1*] **and Toby Sansom**[1]

[1]Inigo Insurance Ltd, 25 Fenchurch Avenue, London, United Kingdom, EC3M 5AD

Abstract

There is a growing appetite for parametric Japanese earthquake insurance products that use Japanese Meteorological Agency seismic intensity, I_{JMA}, triggers. However, most earthquake risk models used to price these contracts do not compute I_{JMA} directly, instead relying on conversions that introduce additional basis risk. Here, we present empirical parameterisations of I_{JMA} as a function of all combinations of moment magnitude, hypocentral distance, peak ground acceleration (PGA), and spectral acceleration (S_a) at 0.2, 0.3, 0.6, 1.0, 2.0, and 3.0 s, derived from earthquake risk model outputs. Parameterisations are fitted using ridge regression applied to 43,002 ground motion recordings from 111 Japanese earthquakes spanning January 2000 to April 2026. A parsimonious two-parameter model — combining PGA and $S_a(1.0\text{ s})$ — outperforms previously published parameterisations, substantially reducing both uncertainty and bias. When applied to a synthetic parametric insurance portfolio exposed to 25 years of Japanese seismicity, this parameterisation yields a measurable reduction in basis risk. These results support more reliable and transparent pricing of parametric earthquake insurance products.

1 Introduction

The Japanese Meteorological Agency (JMA) seismic intensity scale, or Shindo Scale, is a long-established method for categorising the local ground shaking intensity of earthquakes. It was initially devised as a categorical scale, with values assigned by JMA staff based on shaking and damage observations in each location [1]. In 1996, the JMA transitioned to reporting an instrumentally derived seismic intensity (I_{JMA}) which can be converted to the original Shindo Scale [Table 1; 2, 3].

The JMA maintain a dense network of three-component ground-motion accelerometers across Japan that record I_{JMA} and Shindo class for all detectable earthquakes. The speed and reliability of JMA reporting coupled with the objectivity of I_{JMA} calculations make Shindo Scale at the nearest observation point an ideal trigger for parametric earthquake insurance in Japan. Parametric, or index-based, insurance utilises predefined hazard thresholds that trigger payouts representing fixed percentages of the total insured limit [4]. Commonly used hazard triggers within parametric earthquake policies include Peak Ground Acceleration (PGA), Modified Mercalli Intensity, and moment magnitude [M_w; 5, 4, 6]. Parametric products with JMA Shindo Scale triggers are becoming increasingly popular in Japan since I_{JMA} is strongly tied to building damage and payouts can be delivered in a matter of days after an event [7, 8, 9].

Table 1: Conversion between Japanese Meteorological Agency (JMA) instrumentally derived seismic intensity (I_{JMA}) and the traditional classification system (Shindo Scale).

Instrumental Intensity	Shindo Class	Instrumental Intensity	Shindo Class
$I_{\text{JMA}} < 0.5$	0	$4.5 \leq I_{\text{JMA}} < 5.0$	5 lower (5−)
$0.5 \leq I_{\text{JMA}} < 1.5$	1	$5.0 \leq I_{\text{JMA}} < 5.5$	5 upper (5+)
$1.5 \leq I_{\text{JMA}} < 2.5$	2	$5.5 \leq I_{\text{JMA}} < 6.0$	6 lower (6−)
$2.5 \leq I_{\text{JMA}} < 3.5$	3	$6.0 \leq I_{\text{JMA}} < 6.5$	6 upper (6+)
$3.5 \leq I_{\text{JMA}} < 4.5$	4	$I_{\text{JMA}} \geq 6.5$	7

Both buyers and sellers of parametric products desire contractual terms that seek to minimise the difference between insurance payouts and damage incurred, known as basis risk. From the seller's perspective, it is also important to accurately estimate the likelihood that parametric payouts are triggered. Earthquake risk models are commonly utilised by insurers to assess the pricing adequacy of potential deals and manage their exposure to large events [10]. These hazard calculations within these models generally subdivide into earthquake-frequency and ground-shaking-intensity components. Ground motion intensities are typically parameterised as functions of magnitude, hypocentral distance, fault mechanism and site conditions – and several parameterisations

*patrick.ball@inigoinsurance.com

can be used in tandem within a logic tree [11, 12, 13]. Whilst some ground-motion and earthquake-risk models directly estimate I_{JMA} [e.g., 14, 15], it is considerably more common to estimate physical parameters such as PGA and spectral acceleration (S_a) at several periods [e.g., 0.2 s, 0.3 s, 0.6 s, 1 s, 2 s; 12]. Therefore, most earthquake risk model outputs must be converted into I_{JMA} before they can be used to evaluate the parametric insurance deals described above. This conversion step introduces additional basis risk and frequency uncertainty for parametric insurance proposals with Shindo-Scale triggers.

Published empirical relationships exist between several commonly reported ground motion intensity measures and I_{JMA} [16, 17, 18]. However, these models typically draw upon earthquake datasets limited to 20 or fewer events. For applications such as parametric property insurance, where only ground shaking exceeding $I_{\text{JMA}} \approx 5.5$ is relevant, incorporating additional strong-motion observations from more recent large events, such as the 2011 and Tohoku-Oki and 2016 Kumamoto earthquakes, should provide improved relationship fitting. Furthermore, these parameterisations all rely on intensity metrics less commonly calculated by ground motion models, e.g., peak ground velocity, spectral intensity, or the max resultant of peak ground acceleration. In some instances, these differences preclude their usage in insurance contexts, while in others additional basis risk is incurred when converting modelled variables into useable formats.

Here, we present new parameterisations for calculating I_{JMA} that can directly leverage ground motion model outputs. First, we extract and process a wealth of seismic data from across Japan to calculate I_{JMA} and a suite of ground motion intensity metrics typically provided by ground motion models. Second, we employ a multivariate regression approach to develop relationships between these intensity metrics and I_{JMA}. Finally, we apply our chosen I_{JMA} parameterisation to a hypothetical parametric insurance portfolio to demonstrate the reduction of basis risk our new approach provides when compared to previously published parameterisations.

2 EXTRACTION AND PROCESSING OF SEISMIC DATA

The National Research Institute for Earth Science and Disaster Resilience maintain two strong-motion seismographic networks: KiK-Net (Kiban-Kyoshin network) and K-NET [Kyoshin network; 19, 20, 21]. These networks provide dense, ~20 km, coverage across Japan and record three-component waveform data that are made freely available. We extracted ground motion data for 111 earthquakes between 1/1/2000 and 1/4/2026 that are $\geq M_w$ 5.0 and have a recording of ≥ 5.0 I_{JMA} for at least one station (Figure 1a). We only use KiK-Net observations from the surface seismometer and all recordings are corrected using scaling factors provided with the data.

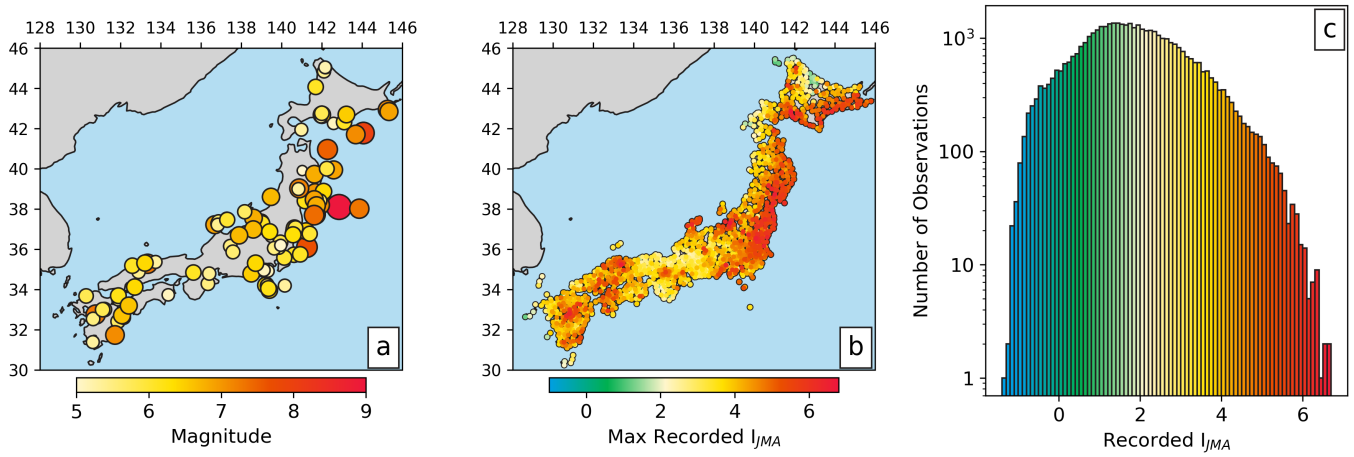

Figure 1: Locations and recorded intensities for 111 $\geq M_w$ 5.0 earthquakes between 1/1/2000 and 1/4/2026 that generate at least one recording ≥ 5.0 I_{JMA}. (a) Locations of processed earthquakes coloured and scaled by their respective magnitudes. (b) K-Net and KiK stations coloured by maximum recorded I_{JMA} value. (c) Histogram of observed I_{JMA} values within our ground motion intensity dataset.

2.1 *Defining and Calculating Ground Motion Intensity Metrics*

Peak ground acceleration (PGA) is the absolute maximum acceleration experienced at a location during an earthquake. Some ground motion models report the geometric mean (GM) of the horizontal components of shaking, whilst others favour the median response when rotated over all horizontal orientations [RotD50; 22]. GM and RotD50 PGA values are defined as

$$\text{PGA}_{\text{GM}} = \max_t \sqrt{a_{\text{NS}}(t) \times a_{\text{EW}}(t)} \tag{1}$$

and

$$\text{PGA}_{\text{RotD50}} = \text{median}_{\theta \in [0,\pi]} \left[\max_t \left(a_{\text{NS}}(t) \cos\theta \times a_{\text{EW}}(t) \sin\theta \right) \right], \tag{2}$$

respectively. Where a is acceleration in the north-south (NS) or east-west (EW) directions as a function of time (t); θ is the rotation angle between 0° and 180°.

Spectral acceleration (S_a) is the maximum acceleration experienced by an idealised damped oscillator with a specified natural period when subjected to ground motion. Typically, S_a is calculated assuming 5% damping and can be expressed at a range of periods including 0.2, 0.3, 0.6, 1.0, 2.0, and 3.0 s. Similarly to PGA, S_a can be presented as both the geometric mean and RotD50 of horizontal ground shaking and both are calculated within this study using the PyRotD python library [23]. All PGA and S_a values are reported in gal.

I_{JMA} is calculated from three-component acceleration time histories [2, 3]. First, three band-pass filters are applied in the frequency domain to isolate the range of ground motions associated with perceptible shaking and potential damage. The filtered components are then combined into a single waveform. From this combined signal, a_0 is taken as the highest acceleration sustained for a minimum duration of 0.3 seconds. Finally, I_{JMA} is computed from a_0 (in cm/s^2) using a logarithmic relationship:

$$I_{\text{JMA}} = \log_{10} a_0 + 9.4. \tag{3}$$

Resulting I_{JMA} values are always reported to one decimal place. This calculation is performed using the shindo.py python library [24].

We calculate PGA, S_a(0.2 s), S_a(0.3 s), S_a(0.6 s), S_a(1.0 s), S_a(2.0 s), S_a(3.0 s) and I_{JMA} for 43,002 strong motion recordings across 111 earthquakes (Figure 1b,c; Supplementary Table 1).

3 Regression Modelling

3.1 Methodology

Our aim is to develop parameterisations for I_{JMA} that are both accurate and simple to operationalise within most insurance pricing workflows. As such, we opt for a regression model and avoid more complex machine-learning approaches, as they often reduce interpretability and can be difficult to operationalise and audit within insurance pricing frameworks. Since not all earthquake risk models provide the same ground motion parameters, we compute several alternative parameterisations to suit most users. The variables we investigate include M_w, the distance between the earthquake hypocentre and recording station (D_{hyp}) and strong ground motion intensities PGA, S_a(0.2 s), S_a(0.3 s), S_a(0.6 s), S_a(1.0 s), S_a(2.0 s), and S_a(3.0 s). Hypocentral distance and strong motion intensities are reported in km and gal, respectively. The relationship between I_{JMA} and maximum acceleration a_0 is log linear and several previous authors have identified log linear relationships between I_{JMA} and both D_{hyp} and ground motion intensities [14, 16, 3]. We therefore assume a regression with the form

$$\min \sum_{i=1}^{n} (y_i - \hat{y}_i)^2 \qquad \text{where} \qquad \hat{y}_i = b_0 + \sum_{j=1}^{1} b_j x_{ij} + \sum_{j=2}^{p} b_j \log_{10}(x_{ij}), \tag{4}$$

regression coefficients b_j are estimated by minimising the squared error between observed and predicted I_{JMA} values (y_i and $\hat{y}_i$, respectively); x_{ij} where $j = 1$ is M_w and x_j where $j > 1$ are D_{hyp} and strong ground motion intensities; p is total number of coefficients.

Parametric insurance contracts typically trigger at $I_{\text{JMA}} \geq 5.5$, where buildings begin to be materially damaged. However, accelerometer recordings that exceed this value only comprise 0.6% of the dataset, which is strongly skewed towards lower I_{JMA} values (see Figure 1c). Since fitting of higher I_{JMA} values is most important for insurance applications and the number of recordings begins to decrease due to seismometer sensitivity limitations at $I_{\text{JMA}} < 2$, we excise all accelerometer recordings with $I_{\text{JMA}} \leq 2$. Remaining I_{JMA} observations are weighted by the inverse of their respective frequencies (f) within the dataset. All weights (w) are normalised so that they have a mean of 1,

$$w_i = \frac{\frac{1}{f(y_i)}}{\frac{1}{n}\sum_{j=1}^{n}\frac{1}{f(y_j)}}. \tag{5}$$

This approach ensures that each I_{JMA} interval contributes equally to the loss function.

Strong multicollinearity may exist between $\log_{10}(\mathrm{PGA})$ and $\log_{10}(S_a)$ at different periods since these variables are all accelerations calculated from the same waveform. Furthermore, both M_w and D_{hyp} may also correlate with ground motion intensities since larger, closer earthquakes tend to cause greater shaking. Including two or more highly correlated variables within a regression increases the variance of their associated coefficients – making them more sensitive to changes in the underlying data, thereby increasing standard error. Figure 2a shows a matrix of Pearson correlation coefficients (R) between each variable and I_{JMA} for recordings where $I_{\mathrm{JMA}} \geq 2$. All strong motion intensity variables show a positive correlation with I_{JMA} ($R \geq 0.55$). However, PGA and S_a with periods between 0.2 s and 1 s are very strongly correlated with each other ($R \geq 0.75$), as are periods between S_a(1.0 s) and S_a(3.0 s).

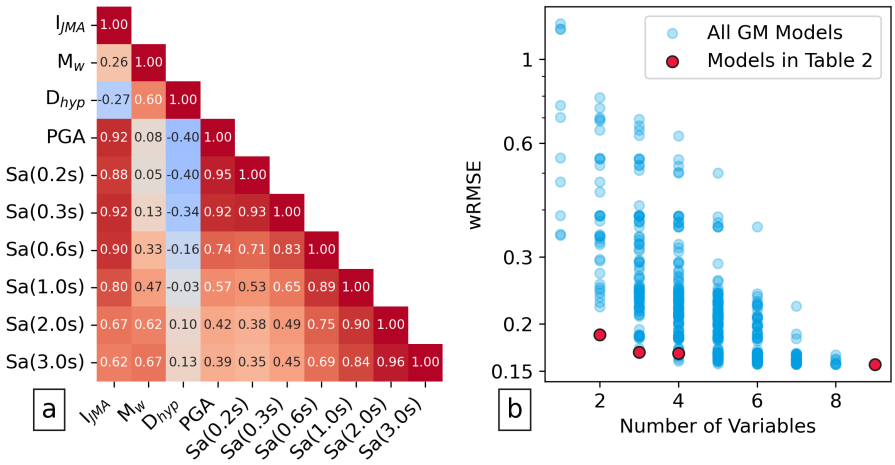

Figure 2: (a) Cross correlation matrix of earthquake observations with $I_{\mathrm{JMA}} \geq 2$ from our earthquake catalogue (Supplementary Table 1). All ground motion intensities are presented as the geometric mean of their horizontal components. Each combination of variables is coloured and annotated with its respective Pearson correlation coefficient. (b) Weighted root mean squared error (wRMSE) as a function of the number of variables in 511 possible regression parameterisations constructed from M_w, $\log_{10}(D_{\mathrm{hyp}})$, $\log_{10}(\mathrm{PGA})$, $\log_{10}(S_a(0.2\ \mathrm{s}))$, $\log_{10}(S_a(0.3\ \mathrm{s}))$, $\log_{10}(S_a(0.6\ \mathrm{s}))$, $\log_{10}(S_a(1.0\ \mathrm{s}))$, $\log_{10}(S_a(2.0\ \mathrm{s}))$, and $\log_{10}(S_a(3.0\ \mathrm{s}))$ with ground motions displayed as geometric means of their horizontal orientations. Blue circles = all parameterisations, red circle = best-fitting models detailed in Table 2.

To mitigate multicollinearity, we employ a ridge regression approach [25]. Ridge regression applies a penalty function that forces coefficients towards zero, thereby reducing overfitting and model instability. All variables are standardised so that their contributions to the penalty function are equally weighted. The adapted regression equation is

$$\min\left(\sum_{i=1}^{n} w_i\,(y_i - \hat{y}_i)^2 + \lambda \sum_{j=1}^{p} b_{ij}^2\right), \tag{6}$$

where b_j represents coefficients for all n variables and λ is the tuning parameter. As λ increases, coefficients are forced closer to zero, decreasing the variance in fit between subsets of sample data but reducing the goodness of fit to the subset of data provided. To select λ, we conduct a search where λ is varied between 0.1 and 1000 and select the λ that provides the lowest weighted root mean squared error (wRMSE) in a five-fold cross validation exercise.

3.2 Regression Results

Our regression methodology is applied to all 511 possible variable combinations drawn from the nine parameters recorded in our database: M_w, D_{hyp}, PGA, S_a(0.2 s), S_a(0.3 s), S_a(0.6 s), S_a(1.0 s), S_a(2.0 s) and S_a(3.0 s). Regressions are computed for parameters derived from both geometric mean and RotD50 horizontal-component orientations, yielding a total of 1,022 candidate

models. Resulting variable coefficients, regularisation parameters, and wRMSE for each model are reported in Supplementary Table 2.

In regression analysis, model fit improves as additional predictor variables are introduced. Akaike and Bayesian Information Criteria are typically calculated to identify the most parsimonious well-performing models, however these metrics become less sensitive to changes in degrees of freedom as the number of samples exceeds a few thousand (Supplementary Table 2). Instead, we compare the wRMSE of all candidate models as a function of the number of included variables (Figure 2b).

Table 2: Each column details meta data and regression coefficients for a possible I_{JMA} parameterisation. Variables = number of variables used in the regression; orientations GM and RotD50 = ground motion intensities calculated as geometric mean and median response of horizontal components, respectively; λ = tuning parameter in ridge regression, wRMSE = weighted root mean squared error; BIC = Bayesian information criterion; all other values are regression coefficients for variables in the left-hand column.

Parameterisation	**P1**	**P2**	**P3**	**P4**	**P5**	**P6**	**P7**	**P8**
Variables	2	2	3	3	4	4	9	9
Orientation	GM	RotD50	GM	RotD50	GM	RotD50	GM	RotD50
λ	521	628	0.1	0.1	187	171	0.1	0.1
wRMSE	0.1870	0.1828	0.1684	0.1669	0.1671	0.1656	0.1563	0.1520
Intercept (b_0)	0.55743	0.3832	0.3491	0.2313	0.3861	0.3178	0.4124	0.3252
M_w							−0.0189	−0.0238
$\log_{10}(D_{\mathrm{hyp}})$							0.0352	0.0407
$\log_{10}(\mathrm{PGA})$	1.27670	1.2815	0.9101	0.9414	0.8814	0.9073	0.9262	0.9986
$\log_{10}(S_a(0.2\ \mathrm{s}))$							0.0063	−0.0495
$\log_{10}(S_a(0.3\ \mathrm{s}))$			0.4570	0.4180	0.4937	0.4591	0.3067	0.2849
$\log_{10}(S_a(0.6\ \mathrm{s}))$							0.3630	0.3798
$\log_{10}(S_a(1.0\ \mathrm{s}))$	0.73264	0.7306	0.6447	0.6548	0.5208	0.5306	0.2681	0.2555
$\log_{10}(S_a(2.0\ \mathrm{s}))$					0.1167	0.1177	0.2048	0.2010
$\log_{10}(S_a(3.0\ \mathrm{s}))$							−0.0488	−0.0379

Resultant parameterisations have wRMSEs ranging from 0.15–1.2 and cluster in two broad groups separated at approximately wRMSE = 0.4. Models in the better performing group (wRMSE < 0.4) all include at least one of PGA, S_a(2.0 s), and S_a(3.0 s) – the variables that most strongly correlate with I_{JMA} (Figure 2a). The best-performing models with 2, 3, 4, and 9 variables that do not rely on S_a(0.6 s) or S_a(3.0 s), which are less commonly calculated by earthquake risk models, are shown in Table 2. The best performing two-variable models achieve wRMSEs approaching that of the nine-variable model (0.1870 and 0.1828 for GM and RotD50, respectively versus 0.1563 and 0.1520; Figure 2b, Table 2). These two-variable solutions employ PGA and S_a(1.0 s), both of which are widely reported by ground motion models. The best-fitting three-variable solutions offer a marginal improvement of fit (0.1684 and 0.1669 for GM and RotD50 orientations, respectively; Figure 2b, Table 2). However, these solutions require S_a(0.3 s), which is less commonly calculated by earthquake risk models than PGA and S_a(1.0 s).

Given the substantial reduction in model complexity alongside the advantage of broad applicability, we select

$$I_{\mathrm{JMA}} = 0.55743 + 1.27690 \times \log_{10}(\mathrm{PGA}_{\mathrm{GM}}) + 0.73264 \times \log_{10}(S_a(1.0\ \mathrm{s})_{\mathrm{GM}}) \tag{7}$$

and

$$I_{\mathrm{JMA}} = 0.38325 + 1.28150 \times \log_{10}(\mathrm{PGA}_{\mathrm{RotD50}}) + 0.73056 \times \log_{10}(S_a(1.0\ \mathrm{s})_{\mathrm{RotD50}}) \tag{8}$$

as our chosen parameterisations (Parameterisations 1 and 2 in Table 2, respectively; hereafter P1 and P2). Nevertheless, all possible solutions are included within Supplementary Table 2, so that users can identify their preferred model based on the variables available from their chosen ground motion or earthquake risk framework.

The performance of P1 at $I_{\mathrm{JMA}} \geq 4.5$ is displayed in Figure 3. There is a strong overall agreement between observed and modelled I_{JMA} values with the majority of points clustering close to the 1:1 line (Figure 3a). Mean residuals for all I_{JMA} values deviate < 0.15 from zero and have tight standard deviations (< 0.25), confirming the model is broadly unbiased (Figure 3b). Standard deviations are largest and a modest tendency towards underprediction is observed when $I_{\mathrm{JMA}} \geq 6$. When I_{JMA} values are binned into Shindo Classes using the conversion illustrated in Table 1, we find that the model correctly identifies the class in 72% and 73% of cases where the observed Shindo classes ≥ 5− and ≥ 6−, respectively (Figure 3c). Misclassifications are restricted to adjacent classes for all but one sample.

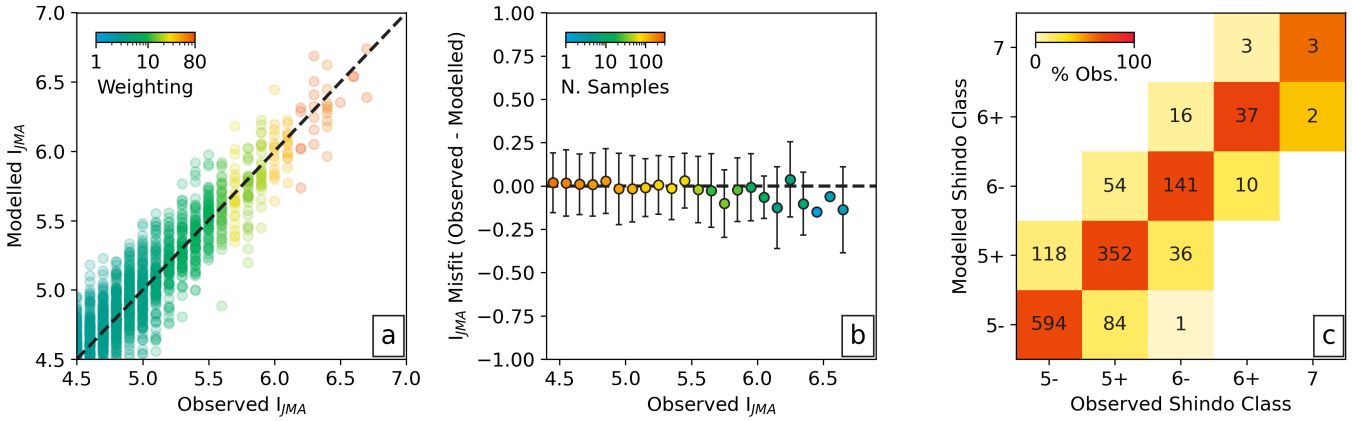

Figure 3: Comparison between observed and modelled I_{JMA} calculated using P1 in Table 2. (a) Modelled I_{JMA} as a function of observed I_{JMA} for all ground motions recordings with observed $I_{\text{JMA}} \geq 4.5$; samples coloured by weighting during regression fitting; dashed line = 1:1 for comparison. (b) Circles and error bars = mean and standard deviation residual misfit between observed and modelled I_{JMA} for all samples in each 0.1 I_{JMA} interval; circles coloured by the number of samples. (c) A comparison between observed and modelled Shindo classes using conversion outlined in Table 1. Number and colour of each bin denotes the count and percentage of observed samples of the class, respectively.

4 Discussion

4.1 Comparison to an Established Parameterisation

To assess the performance of our parameterisation we compare its predictive power to a commonly used published alternative by Karim and Yamazaki [16]; hereafter KY02. Several parametrisations are presented by KY02, however, only Equation 14 in that paper does not rely on peak ground velocity or spectral intensity, and can therefore be implemented using the output from most contemporary earthquake risk models, such as the Global Earthquake Model [12]. Equation 14 in KY02 estimates that

$$I_{\text{JMA}} = -0.65 + 0.18 \times M_w + 1.81 \times \log_{10}(\text{PGA}_R), \tag{9}$$

where PGA_R is the maximum resultant horizontal PGA. Applying this parameterisation to our ground motion database yields a wRMSE of 0.3583 (Figure 4a,b). This performance is substantially poorer than both our chosen parameterisation and is similar to our equivalent regression fitted using only M_w and PGA terms (wRMSE = 0.33; Supplementary Table 2). Mean residuals for each I_{JMA} value can diverge from zero by up to 0.22 whilst most standard deviations exceed 0.25 (Figure 4a). These uncertainties propagate into greater misclassifications of Shindo classes, particularly for damaging shaking levels (44% of cases where the observed class is ≥ 5−; 41% when the observed class is ≥ 6− Figure 4b).

A practical limitation of KY02 is that most earthquake risk models do not directly output PGA_R. Instead, they provide PGA_{GM} or $\text{PGA}_{\text{RotD50}}$, and so an additional conversion step is typically required before KY02 can be applied. Recordings with $I_{\text{JMA}} \geq 2$ in our ground motion dataset have a mean conversion factor of 1.5835 between PGA_R and PGA_{GM}. Using this conversion elicits broadly similar results to using observed PGA_R values directly (wRMSE = 0.3595; Figure 4c,d).

Since PGA_R sits within KY02's logarithmic term, small differences in a PGA_{GM}–PGA_R conversion factor can strongly influence parameterisation performance – and published conversions vary considerably. For example, Karim and Yamazaki [16] provide a conversion factor of 1.068 between PGA of the larger of the two horizontal coordinates (PGA_L) and PGA_R. Combining this PGA_L–PGA_R factor with a PGA_L–PGA_{GM} factor from Campbell and Bozorgnia [26], yields a resultant conversion factor of 1.193. Using 1.193 leads to modelled underestimates of I_{JMA} that increase from ~0.05 to ~0.35 as observed I_{JMA} values rise from 4.5 to 6.5 (Figure 4e). As a result, only 44%, 36%, and 20% of observations with Shindo Classes of 6−, 6+ and 7 are correctly identified, respectively; with the majority of misclassifications being underestimates (Figure 4f). These results demonstrate that parameterisations that require intermediate conversions of ground-motion terms can introduce potentially significant bias and uncertainty for I_{JMA} estimates that can have downstream impacts on basis risk and insurance decision making.

4.2 Pricing an Illustrative Synthetic Insurance Portfolio

To demonstrate how uncertainties in I_{JMA} parameterisation propagate into insured losses, we apply observed and parameterised I_{JMA} observations between January 2000 and April 2026 to a synthetic parametric insurance portfolio. This synthetic portfolio

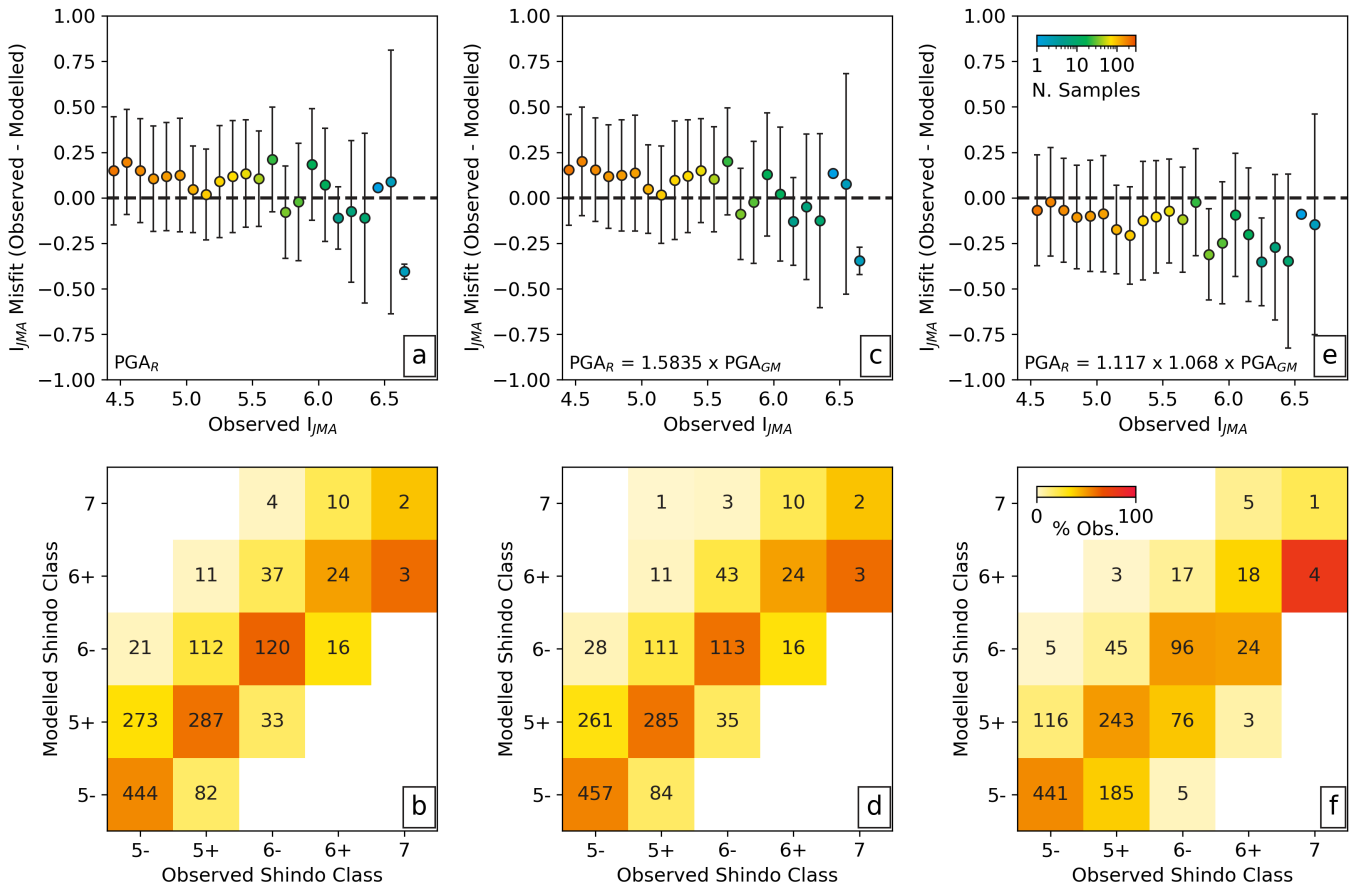

Figure 4: Comparison between observed and modelled I_{JMA} calculated using Equation 14 in Karim and Yamazaki [16]. (a) Circles and error bars = mean and standard deviation residual misfit between observed and modelled I_{JMA} for all samples in each 0.1 I_{JMA} interval; circles coloured by the number of samples. (b) A comparison between observed and modelled Shindo classes using conversion outlined in Table 1. Number and colour of each bin denotes the count and percentage of observed samples of the class denoted by the X axis in the bin, respectively. (c and d) Same as 4a and b, respectively with a conversion between PGA_R and $\mathrm{PGA}_{\mathrm{GM}}$ defined in lower left of 4c. (e and f) Same as 4a and b, respectively, using a conversion between PGA_R and $\mathrm{PGA}_{\mathrm{GM}}$ defined in lower left of 4e [26, 16].

combines healthcare facilities and power stations across Japan drawn from two publicly available datasets [27, 28, ; Supplementary Table 3]. Both asset classes serve critical social functions, have incurred losses during historic Japanese earthquakes, and could conceivably have parametric earthquake coverage [29, 30, 31, 32]. By combining healthcare and power facilities, we hope to reflect the broad distribution of Japan's population and industry whilst providing reasonable coverage of its diverse earthquake risk and experience (Figure 5a).

Table 3: Parametric payout structure representing the percentage of the total insured value (10 billion JPY) that is paid to the insured in the event of an earthquake causing a Shindo intensity at or above the given thresholds at the nearest KiK or K-Net seismic station if one is located within 20 km at the time of the event.

Shindo Class	5 Upper (5+)	6 Lower (6−)	6 Upper (6+)	7
I_{JMA}	$5.0 \leq I_{\mathrm{JMA}} < 5.5$	$5.5 \leq I_{\mathrm{JMA}} < 6.0$	$6.0 \leq I_{\mathrm{JMA}} < 6.5$	$I_{\mathrm{JMA}} \geq 6.5$
Payout (%)	12.5%	25%	50%	100%

We apply a parametric payout structure to each asset that attaches at a Shindo Scale value of 5+ and pays the full insured value if Shindo Scale reaches 7 (Table 3). This structure is reflective of existing formats in the market [7, 9]. In each earthquake, every asset is assigned the Shindo scale recorded at the closest K-Net or KiK station that was operational during the event, with a maximum seismometer-location distance of 20 km. All assets are allotted uniform insured values, or limits, of 10 billion JPY to create a 'flat portfolio' where limits are decoupled from true asset values. This normalisation removes confounding differences in underlying asset value to isolate the effect of I_{JMA} parameterisation.

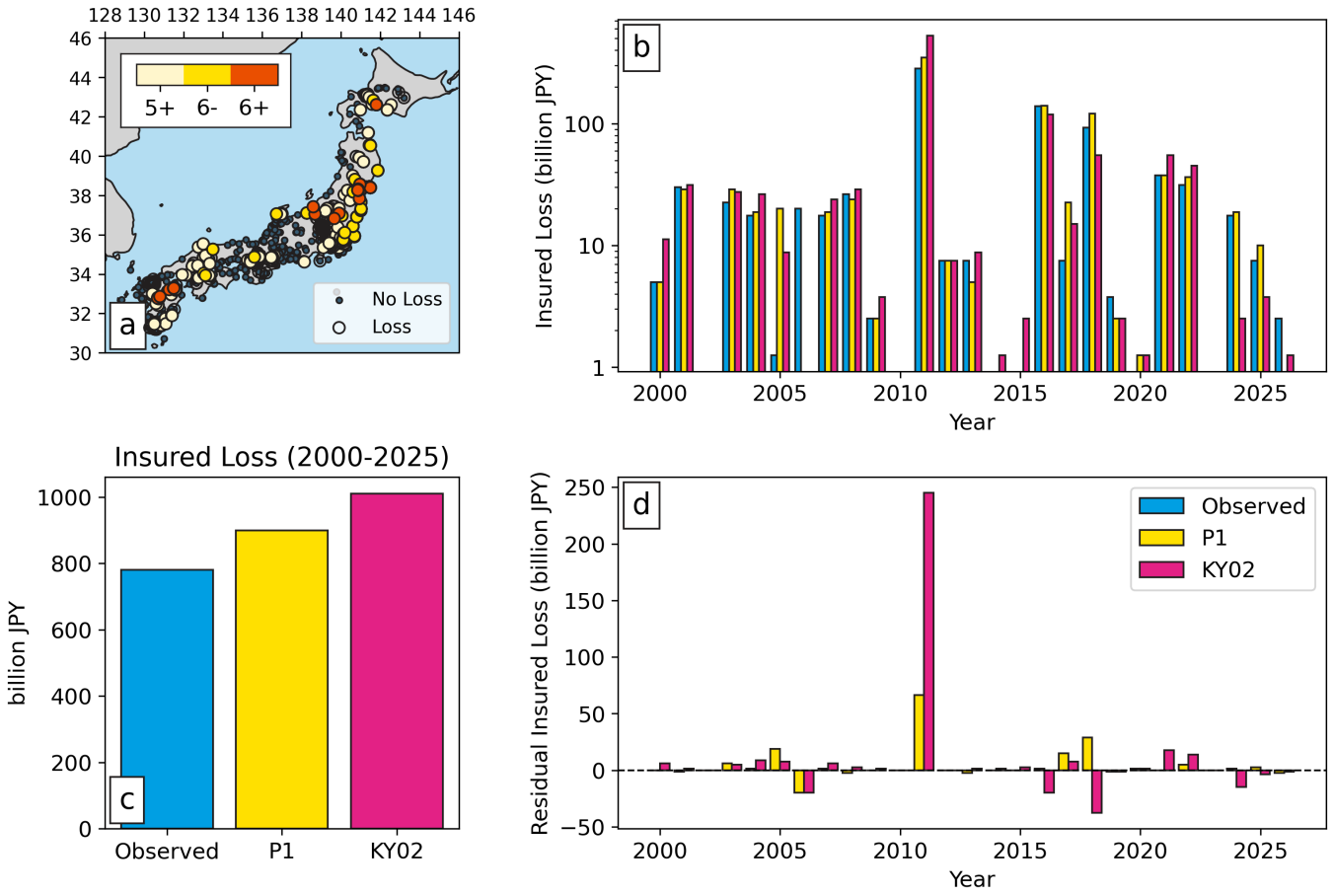

Figure 5: Application of I_{JMA} parameterisations to a synthetic parametric insurance portfolio using real events between 2000 and 2026 (Supplementary Table 1). (a) Locations within the synthetic portfolio; small and large circles are untriggered and triggered locations, respectively. Triggered locations coloured by the largest Shindo Scale experienced. (b) Loss experience time series; blue, yellow and pink bars show annual insured losses calculated using Shindo Class observations, those estimated using P1 and those calculated using KY02, respectively. (c) Aggregated losses for all events between 2000 and 2025; colours are the same as Figure 5b. (d) Annual loss differences using Shindo Scale observations and parameterisation, positive values are parameterisation overestimates.

We subject our synthetic portfolio to all 111 historic earthquakes in our ground motion catalogue using observed I_{JMA} values, and those calculated using P1 and KY02. Total insured losses incurred by the synthetic portfolio each year using each I_{JMA} parameterisation are shown in Figure 5b. Losses calculated using observed intensities exceed 100 billion JPY in three major earthquake years: the 2011 Tohoku-Oki, 2016 Kumamoto and 2018 Osaka earthquakes. Together, these three years represent 66% of the 780 billion JPY total aggregate insured loss (Figure 5c). Both I_{JMA} parameterisations overestimate aggregate losses compared to observations but the bias differs substantially. P1 and KY02 increase aggregate losses by 15% and 29%, respectively (Figure 5c). KY02 also generates larger, and more frequent annual residual losses, with annual loss misfits exceeding 5 billion JPY in 12 years compared to 6 years using P1 (Figure 5d). In a parametric insurance context, these discrepancies represent higher basis risk.

Aggregate loss overestimates for both parameterisations are primarily driven by the M_w 9.0 Tohoku-Oki earthquake, the largest recorded earthquake and largest insurance loss in Japanese history [Figure 5d; 33]. For the Tohoku-Oki earthquake, KY02 overestimates losses for 106 locations across a region north of ~35.6°N and underestimates losses for a smaller cluster of 14 locations around Tokyo Bay (Figure 6a). In contrast, P1 yields a much smaller residual loss, less strong spatial clustering, and a more even split between over- and underestimated locations (27 and 9 locations, respectively; Figure 6b). These spatial and residual differences are likely linked to how each parameterisation captures local site conditions and their influence on ground motions, as well as the extreme nature and magnitude of the Tohoku-Oki earthquake.

Parameterisations of I_{JMA} that include peak ground velocity or spectral intensity terms generally outperform those based solely on PGA and M_w [16, 3]. Our results suggest that this improvement primarily reflects the inclusion of terms that respond to local

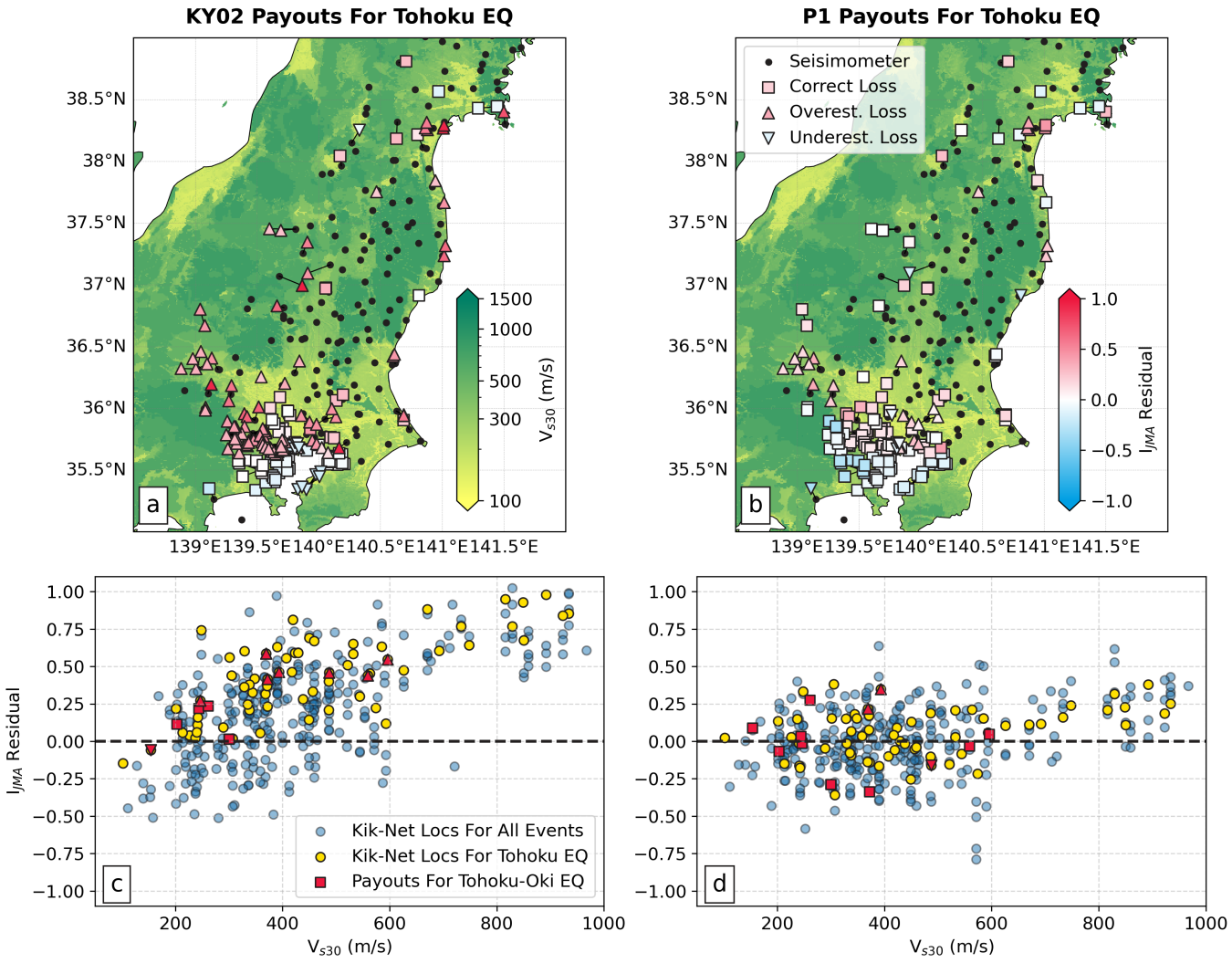

Figure 6: Parameterisation performance for the Tohoku-Oki Earthquake, 2011. (a) Map of Tohoku-Oki-earthquake-affected region with background grid coloured by V_{s30} value [34]. Inverted-triangles, squares, and triangles are insured locations where triggered losses in the synthetic portfolio are under-, correctly and over-estimated using KY02, respectively. Symbols are coloured by the residual misfit between parameterised and observed I_{JMA} and black lines tie insured locations to their nearest seismometer. Black dots are locations of seismometers with Tohoku-Oki earthquake ground motion intensity recordings (Supplementary Table 1). (b) Same as Figure 6a with I_{JMA} values calculated using P1. (c) Difference between observed and parameterised KiK-net station I_{JMA} values $\geq$ 4.5 using Equation 14 in Karim and Yamazaki [16] as a function of V_{s30} values provided by Zhu et al. [35]. Blue circles are all seismometer recordings for all earthquakes in Supplementary Table 1; yellow circles are recordings for Tohoku-Oki earthquake; red inverted-triangles/squares/triangles are recordings that trigger losses in the synthetic portfolio that are under-/correctly/over-estimated using KY02. (d) Same as Figure 6c but parameterised I_{JMA} calculated using P1 in Table 2.

site conditions, such as the stiffness of the subsurface. Near-surface stiffness is commonly quantified by the average shear-wave velocity within the top 30 m of the subsurface (V_{s30}). Softer sediments (i.e., lower V_{s30}) typically amplify seismic shaking as incoming shear waves decelerate as they enter lower stiffness materials. This amplification response varies considerably depending on the amplitude and frequency of incoming shear waves and the stiffness profile of the subsurface. During stronger shaking in soft sediments, higher frequency waves (e.g., S_a 0.1–0.3 s) can become increasingly damped whilst lower frequency waves (e.g., S_a 1.0–3.0 s) continue to amplify [36]. I_{JMA} is sensitive to a broad range of frequencies, whereas PGA is dominated by the highest-frequency components of shaking. Consequently, parameterisations relying solely on PGA struggle to reproduce the full site response captured by I_{JMA}.

To evaluate this effect, we compare observed and parameterised I_{JMA} values for KiK-Net recordings with $I_{\text{JMA}} \geq 4.5$ as a function of V_{s30} [Supplementary Table 1; 35]. We confine our analysis to KiK-Net stations since their paired surface and borehole seismometers

provide a more accurate estimate of V_{s30} than the surface-only K-Net network [20, 35]. There is a strong positive correlation between V_{s30} and residual misfit between observed I_{JMA} and those calculated using KY02 for both the Tohoku-Oki earthquake and the full observational record (Figure 6c). This parameterisation systematically underestimates shaking in soft-sediment environments, including the margins of Tokyo Bay, while overestimating shaking at stiffer sites further north.

P1 substantially reduces this V_{s30}-dependent bias (Figure 6d). The inclusion of both PGA and S_a(1.0 s) terms better captures the combined influence of high- and low-frequency shaking on I_{JMA}. However, a slight increase in residual misfit remains at $V_{s30} \geq 600$ m/s since these two terms alone do not capture the full site response. Where practical, researchers may seek to use Parameterisations 3–6 in Table 2, that include S_a(2.0 s) and S_a(3.0 s) terms, which may reduce basis risk.

In addition to its sensitivity to V_{s30}, KY02 produces systematically larger overestimates of I_{JMA} for the Tohoku-Oki earthquake compared to other events with comparable site conditions (Figure 6c). This overestimate may stem from the large magnitude of the Tohoku-Oki earthquake and the inclusion of M_w as a direct additive within the KY02 parameterisation (Equation 9). Because M_w is an event-level property rather than a site-specific measure of shaking, its inclusion can introduce non-physical behaviour at large magnitudes or low levels of shaking. For example, if a station records no shaking for the Tohoku-Oki earthquake, the KY02 parameterisation will estimate an I_{JMA} of ~1 solely due to the M_w term. This effect becomes more important for larger earthquakes with distal observations. P1 avoids this issue since it relies exclusively on ground-motion intensity metrics. Consequently, the residual misfits for the Tohoku-Oki earthquake are evenly distributed around zero and are of similar absolute values to the rest of the observational dataset (Figure 6d).

4.3 Implications for Future Parametric Insurance Contracts

Our I_{JMA} parameterisations should reduce basis risk compared to KY02, so that underwriting and pricing teams can construct and evaluate I_{JMA}-based parametric policies with greater confidence. This may encourage broader acceptance of such structures across both insurance and reinsurance markets, and support wider uptake of I_{JMA} as a principal trigger index. However, basis risk remains unavoidable when using parametric earthquake triggers. In practice, it arises from multiple sources including shaking differences between insured locations and reference seismometers, deviations between incurred damages and triggered payouts, as well as the uncertainties derived from the earthquake risk model used to price the contract. Nevertheless, basis risk can be mitigated by thoughtful payout-structure design [37]. For example, using 0.1 increments of I_{JMA} in place of steps in Shindo Class can mitigate thresholding effects and avoid large loss changes [e.g., 9]. Although increasing the number of steps can reduce the interpretability of the product, potential policy holders tend to prefer products that demonstrably reduce basis risk [38]. In addition, our simple synthetic example assumes that all hospitals and power plants have equal values and vulnerabilities. Detailed understanding of an asset's underlying risk (e.g., its structural vulnerability and historical damage) can improve the tailoring of an insurance policy and reduce basis risk.

Using I_{JMA} as a parametric insurance trigger introduces an additional modelling step compared to more common approaches such as PGA or M_w within a given distance. However, these simpler triggers can themselves produce substantial basis risk because they are poorer predictors of damage that do not adequately represent site amplification and frequency-dependent effects [39]. These issues are particularly important for structures on very soft or very stiff soils, or for buildings that are more vulnerable to lower-frequency shaking. The Modified Mercalli Intensity (MMI) scale offers a closer analogue to I_{JMA}, as it has been developed to reflect observed damage [40]. However, MMI lacks instrumental objectivity, relying on observational reports in its derivation. Furthermore, PGA and MMI do not carry the same societal familiarity across Japan as I_{JMA}, which is embedded in public emergency broadcasting [41]. As such, the close association between I_{JMA} and damage, its established meaning across Japanese society, and the objectivity of its calculation make it a beneficial trigger for both buyers and sellers of parametric earthquake products.

More broadly, the parametric insurance market would benefit from wider adoption of instrumentally-derived intensity metrics that incorporate multiple spectral frequencies and align more closely with observed damage. Beyond I_{JMA}, promising candidates include spectral intensity, average spectral acceleration, and filtered incremental velocity, which could serve as effective triggers in other seismic settings [39, 42]. The methodology presented here provides a transferable framework for estimating any such metric from earthquake-model output, subject to the availability of sufficient observational data for calibration. Wider adoption of such indices could improve both the reliability and affordability of parametric earthquake (re)insurance globally — particularly in regions where large parametric policies serve as the primary financial protection for uninsured populations and public assets.

5 CONCLUSIONS

A suite of parameterisations has been constructed that estimate I_{JMA} from a variety of earthquake parameters and ground motion intensity metrics (Supplementary Table 2). These parameterisations are fitted to and evaluated with a large dataset of Japanese ground motion observations recorded between 2000 and 2026 (Supplementary Table 1). Of these, we select P1 in Table 2 as our most parsimonious well-fitting solution and compare its performance to observed I_{JMA} values and those calculated using a previously published method [16]. We find P1 reduces misfit to observed I_{JMA} recordings compared to published approaches,

particularly if users are constrained to the output of earthquake risk models. We believe this parameterisation will prove useful for both the earthquake risk and parametric insurance communities.

6 ACKNOWLEDGEMENTS

PWB and TS are supported by Inigo Insurance. We are grateful to A. Alvarez, T. Kang, L. Nicotina, R. Petrie, D. Smith, and A. Starr for their help. We thank NEID for recording and freely providing the seismic data used in this analysis [21]. Figures were prepared using matplotlib [43].

DATA AND CODE AVAILABILITY

Processed seismic data and parameterisation results available in Supplementary Tables 1 and 2, respectively. All codes used in the creation of this paper are available at https://doi.org/10.5281/zenodo.20493491 [44].

COMPETING INTERESTS

None

REFERENCES

[1] Tatsuo Hirono and Katsumi Sato. MSK intensity scale as compared with jma intensity scale. *Papers in Meteorology and Geophysics*, 22(3–4):177–193, 1971. doi: 10.2467/mripapers1950.22.3-4_177.

[2] Junji Kiyono, Kazuki Fujie, and Yutaka Ohta. A combined instrumental seismic intensity – concept, formulation and application. *Doboku Gakkai Ronbunshu*, 612:143–151, 1999.

[3] Saburoh Midorikawa, Kohji Fujimoto, and Issei Muramatsu. Correlation of new J.M.A. instrumental seismic intensity with former J.M.A. seismic intensity and ground motion parameters. *Journal of the Institute of Social Safety Science*, 1:51–56, 1999.

[4] DJ Wald and G Franco. Financial decision-making based on near-real-time earthquake information. In *Proceedings of the 16th world conference on earthquake engineering*, pages 1–13. Santiago de Chile Chile, 2017. URL http://www.wcee.nicee.org/wcee/article/16WCEE/WCEE2017-3625.pdf.

[5] Wolfgang K. Härdle and Brenda L. Cabrera. Calibrating cat bonds for mexican earthquakes. *Journal of Risk & Insurance*, 77 (3):625–650, 2010. doi: 10.1111/j.1539-6975.2010.01355.x.

[6] Hamish K. Mistry and Denis Lombardi. Pricing risk-based catastrophe bonds for earthquakes at an urban scale. *Scientific Reports*, 12:9729, 2022. doi: 10.1038/s41598-022-13588-1.

[7] Masao Iwasaki. Customer case study: Parametric quake japan. https://corporatesolutions.swissre.com/insights/knowledge/customer-case-study-parametric-quake-japan.html, 2021. Accessed: 2026-04-30.

[8] J. Willard. Hdi global se & descartes receive approval to provide parametric earthquake insurance in japan. https://www.artemis.bm/news/hdi-global-se-descartes-receive-approval-to-provide-parametric-earthquake-insurance-in-html, 2025. Accessed: 2026-04-30.

[9] Descartes Underwriting. Ensuring resilience in japan with parametric earthquake solutions. https://descartesunderwriting.com/case-studies/ensuring-resilience-japan-parametric-earthquake-solutions, 2025. Accessed: 2026-05-26.

[10] Anirudh Rao, Catalina Yepes-Estrada, Kendra Johnson, Lana Todorović, Marco Pagani, Michele Simionato, Richard Styron, Vitor Silva, and Helen Crowley. Evolution of the openquake engine: Enhanced capabilities, collaborative development, and global adoption. *Earthquake Spectra*, 41(5):3299–3336, 2025.

[11] Vitor Silva, Desmond Amo-Oduro, Alejandro Calderon, Cristina Costa, Jamal Dabbeek, Venetia Despotaki, Luis Martins, Marco Pagani, Anirudh Rao, Marco Simionato, Daniele Viganò, Catalina Yepes-Estrada, Ana Acevedo, Helen Crowley, Nick Horspool, Kishor Jaiswal, Murray Journeay, and Massimiliano Pittore. Development of a global seismic risk model. *Earthquake Spectra*, 36(1):372–394, 2020. doi: 10.1177/8755293019899953.

[12] Hiroyuki Fujiwara, Nobuyuki Morikawa, Takahiro Maeda, Asako Iwaki, Shunsuke Senna, Shinichi Kawai, Hiroshi Azuma, Xiaoqian Hao, Masajiro Imoto, Kazue Wakamatsu, Jun'ichi Miyakoshi, Tetsushi Morii, Nobuyuki Shimazu, Masahiro Takahashi, and Masashi Akatsuka. Psha input model documentation for japan (jpn). Technical report, Global Earthquake Model, 2023.

[13] Morgan P Moschetti, Brad T Aagaard, Sean K Ahdi, Jason Altekruse, Oliver S Boyd, Arthur D Frankel, Julie Herrick, Mark D Petersen, Peter M Powers, Sanaz Rezaeian, et al. The 2023 us national seismic hazard model: Ground-motion characterization for the conterminous united states. *Earthquake Spectra*, 40(2):1158–1190, 2024.

[14] Kenneth W. Campbell and Yousef Bozorgnia. A ground motion prediction equation for jma instrumental seismic intensity for shallow crustal earthquakes in active tectonic regimes. *Earthquake Engineering & Structural Dynamics*, 40(4):413–427, 2011. doi: 10.1002/eqe.1027.

[15] Earthquake Research Committee. Report: National seismic hazard maps for japan (2020) map edition. Technical report, Headquarters for Earthquake Research Promotion, 2021. URL https://www.jishin.go.jp/main/chousa/26jan_yosoku-e/index-e.htm.

[16] Kazi Rezaul Karim and Fumio Yamazaki. Correlation of jma instrumental seismic intensity with strong motion parameters. *Earthquake Engineering & Structural Dynamics*, 31(5):1191–1212, 2002. doi: 10.1002/eqe.158.

[17] Kohji Fujimoto and Saburoh Midorikawa. Empirical relationship between jma instrumental seismic intensity and ground motion parameters considering the effect of earthquake magnitude. *Journal of Japan Association for Earthquake Engineering*, 10(2):1–11, 2010. doi: 10.5610/jaee.10.2_1.

[18] Florin Pavel and Alexandru Aldea. I_{JMA}-based evaluation of ground motion recordings from Vrancea intermediate-depth earthquakes. *Bulletin of Earthquake Engineering*, 23:4285–4303, 2025. doi: 10.1007/s10518-025-02220-y.

[19] Shin Aoi, Takashi Kunugi, and Hiroyuki Fujiwara. Strong-motion seismograph network operated by nied: K-net and kik-net. *Journal of Japan Association for Earthquake Engineering*, 4(3):65–74, 2004. doi: 10.5610/jaee.4.3_65.

[20] Shin Aoi, Takashi Kunugi, Hiroki Nakamura, and Hiroyuki Fujiwara. Deployment of new strong motion seismographs of K-NET and KiK-net. In *Earthquake Data in Engineering Seismology*, Geotechnical, Geological, and Earthquake Engineering, pages 167–186. Springer, Dordrecht, 2010. doi: 10.1007/978-94-007-0152-6_12.

[21] National Research Institute for Earth Science and Disaster Resilience. K-net, kik-net. Dataset, 2019. URL https://doi.org/10.17598/NIED.0004.

[22] David M. Boore. Orientation-independent, nongeometric-mean measures of seismic intensity from two horizontal components of motion. *Bulletin of the Seismological Society of America*, 100(4):1830–1835, 2010. doi: 10.1785/0120090400.

[23] Albert Kottke, Kris Vanneste, and Stef Bot. arkottke/pyrotd: v0.6.1, 2023. URL https://doi.org/10.5281/zenodo.8101955.

[24] RR-Inyo. shindo: Calculates JMA (Japan Meteorological Agency) seismic intensity (shindo) scale from acceleration data recorded in NumPy array. https://github.com/RR-Inyo/shindo, 2021. URL https://github.com/RR-Inyo/shindo. Accessed: 2026-06-01.

[25] Arthur E. Hoerl and Robert W. Kennard. Ridge regression: Applications to nonorthogonal problems. *Technometrics*, 12(1):69–82, 1970. doi: 10.1080/00401706.1970.10488646.

[26] Kenneth W. Campbell and Yousef Bozorgnia. Campbell–Bozorgnia NGA ground motion relations for the geometric mean horizontal component of peak and spectral ground motion parameters. PEER Report 2007/02, Pacific Earthquake Engineering Research Center, 2007.

[27] Logan Byers, Johannes Friedrich, Roman Hennig, Aaron Kressig, Xinyue Li, Laura Malaguzzi Valeri, and Colin McCormick. A global database of power plants. Technical note, World Resources Institute, 2018. URL https://www.wri.org/research/global-database-power-plants.

[28] Healthsites.io. The global healthsites mapping project. https://healthsites.io/, 2026. Open healthcare facility dataset and API. Accessed: 2026-05-29.

[29] KC Kuo, Yasuhiro Hayashi, and Hiroshi Kambara. Relationship between damages of hospital facilities and seismic intensity based on questionnaire survey. *J. Struct. Constr. Eng. AIJ*, 586:63–69, 2004. doi: https://doi.org/10.3130/aijs.69.63_6.

[30] Phillip Y Lipscy, Kenji E Kushida, and Trevor Incerti. The fukushima disaster and japan's nuclear plant vulnerability in comparative perspective. *Environmental science & technology*, 47(12):6082–6088, 2013. doi: https://doi.org/10.1021/es4004813.

[31] O Ohlmeyer, M Hotz, and A Martin. Parametric enables nepal's renewable energy project financing. https://corporatesolutions.swissre.com/insights/knowledge/parametric-renewable-energy-nepal.html, 2023. Accessed: 2026-05-26.

[32] CCIRF SPC. Annual report 2024-2025. Technical report, The Caribbean Catastrophe Risk Insurance Facility, 2025. URL https://www.ccrif.org/sites/default/files/publications/annualreports/CCRIF-SPC-Annual-Report-2024_2045_web.pdf.

[33] Yoshio Kajitani, Stephanie E. Chang, and Hirokazu Tatano. Economic impacts of the 2011 tohoku-oki earthquake and tsunami. *Earthquake Spectra*, 29(S1):457–478, 2013. doi: 10.1193/1.4000108.

[34] Daniel C. Heath, David J. Wald, C. Bruce Worden, Eric M. Thompson, and Gregory M. Smoczyk. A global hybrid V_{S30} map with a topographic slope-based default and regional map insets. *Earthquake Spectra*, 36(3):1570–1584, 2020. doi: 10.1177/8755293020911137.

[35] Chuanbin Zhu, Marco Pilz, and Fabrice Cotton. Which is a better proxy, site period or depth to bedrock, in modelling linear site response in addition to the average shear-wave velocity? *Bulletin of Earthquake Engineering*, 18:797–820, 2020. doi: 10.1007/s10518-019-00738-6.

[36] Emel Seyhan and Jonathan P Stewart. Semi-empirical nonlinear site amplification from nga-west2 data and simulations. *Earthquake Spectra*, 30(3):1241–1256, 2014. doi: https://doi.org/10.1016/j.soildyn.2014.08.015.

[37] Laura Calvet, Madeleine Lopeman, Jésica de Armas, Guillermo Franco, and Angel A Juan. Statistical and machine learning approaches for the minimization of trigger errors in earthquake catastrophe bonds. *Statistics and Operations Research Transactions*, pages 373–392, 2017. doi: http://doi.org/10.2436/20.8080.02.64.

[38] Ghada Elabed, Marc F. Bellemare, Michael R. Carter, and Catherine Guirkinger. Managing basis risk with multiscale index insurance. *Agricultural Economics*, 44:419–431, 2013. doi: 10.1111/agec.12025.

[39] Hao Wu, Kazuaki Masaki, Kojiro Irikura, Koichiro Saguchi, Susumu Kurahashi, and Xin Wang. Relationship between building damage ratios and ground motion characteristics during the 2011 tohoku earthquake. *Journal of Natural Disaster Science*, 34(1):59–78, 2012.

[40] David J Wald, Vincent Quitoriano, Thomas H Heaton, and Hiroo Kanamori. Relationships between peak ground acceleration, peak ground velocity, and modified mercalli intensity in california. *Earthquake spectra*, 15(3):557–564, 1999.

[41] Japan Meteorological Agency and Cabinet Office of Japan. On the launch of the estimated seismic intensity distribution map service. Technical report, Japan Meteorological Agency, February 2004. URL https://www.jma.go.jp/jma/press/0402/26a/sindo040226.pdf. Press release. Accessed: 2025.

[42] Vitor A Monteiro, Savvinos Aristeidou, and Gerard J O'Reilly. Spatial cross-correlation models for next-generation amplitude and cumulative intensity measures. *Earthquake Spectra*, 42(2):e70076, 2026.

[43] J. D. Hunter. Matplotlib: A 2d graphics environment. *Computing in Science & Engineering*, 9(3):90–95, 2007. doi: 10.1109/MCSE.2007.55.

[44] P.W. Ball and T. Sansom. paddywballinigo/ball_sansom_26: Ps26_submitted (ps26_submitted). https://doi.org/10.5281/zenodo.20493491, 2026. Accessed: 2026-06-01.

Supplementary Materials: Empirical Relationships Between Ground Motion Intensities and JMA Seismic Intensity Scale

Non-peer-reviewed preprint submitted to EarthArXiv, compiled June 4, 2026

Patrick W. Ball[1*] **and Toby Sansom**[1]

[1]Inigo Insurance Ltd, 25 Fenchurch Avenue, London, United Kingdom, EC3M 5AD

1 Supplementary Table 1

Supplementary Table 1 contains 43,002 strong motion recordings across 111 Japanese earthquakes from the National Research Institute for Earth Science and Disaster Resilience maintain two strong-motion seismographic networks: KiK-Net (Kiban-Kyoshin network) and K-NET [Kyoshin network; 1]. These earthquakes were recorded between 1/1/2000 and 1/4/2026, are $\geq M_w$ 5.0, and have a recording of $\geq$ 5.0 I_{JMA} for at least one station. We only use K-Net observations from the surface seismometer and all recordings are corrected using scaling factors provided with the data. The following columns are included in the table:

- Origin_Time - the date and time the earthquake occurred.
- EQ_Longitude, EQ_Latitude, EQ_Depth_km - location of earthquake hypocenter.
- Magnitude - earthquake moment magnitude.
- Network - network of recording station (kik or knet).
- Station_Code - station identifying code.
- Station_Longitude, Station_Latitude, Station_Height_m - Location of recording station
- Record_Time - the date and time the recording was taken.
- Max_Acc_gal, Max_h_Acc_gal - maximum peak ground acceleration recorded as the resultant in 3-component and horizontal directions.
- Geom_h_PGA_gal, Rot50_h_PGA_gal - Geometric mean (Geom) and RotD50 (Rot50) horizontal peak ground acceleration.
- Geom_h_SaX_gal, Rot50_h_SaX_gal - Geometric and RotD50 mean horizontal spectral acceleration (Sa) with 5% damping where X is 0.2, 0.3, 0.6, 1.0, 2.0 or 3.0 s.
- Shindo_Intensity - Japanese Meteorological Agency seismic intensity value.

This table was constructed using Strong_Motion_Data_Processing.ipynb which leverages the PyRotD and shindo.py python libraries [2, 3]. All PGA and S_a values are reported in gal.

2 Supplementary Table 2

Supplementary Table 2 contains the best-fitting regression model coefficients for all possible combinations of the input parameters (see Regression Modelling, Methodology in main text). Column headers include the variable associated with each coefficient. These are:

- intercept - the Y-axis intercept.
- M_w - moment magnitude of the earthquake.
- log10_D_{hyp} - the log of the distance between the hypocenter and the recording station.
- log10_PGA - the log of peak ground acceleration.
- log10_Sa_X - the log of spectral acceleration at X period, where X is 0.2, 0.3, 0.6, 1.0, 2.0, or 3.0 s.

Hypocentral distances and strong motion observations are presented in km and gal, respectively. All strong motion parameters can be presented as the geometric means of their horizontal components (GM) or as the median response when rotated over all horizontal orientations (RotD50). Metadata provided includes:

*patrick.ball@inigoinsurance.com

- Orientation - the orientation of strong motion parameters, GM or RotD50.
- Degrees_of_Freedom - the number of regression parameters considered.
- lamda - the regularisation parameter.
- wRSME - weighted root-mean-squared error.
- BIC - Bayesian Information Criterion.
- Effective_Degrees_of_Freedom - effective degrees of freedom.

To aid model comparison, we calculate each parameterisation's Bayesian Information Criterion (BIC) to evaluate their respective performance whilst penalising unnecessary model complexity [4]. In a regression analysis, the goodness of fit will always improve when an additional variable is introduced. Since Ridge regression regularises coefficients toward zero, the model is less complex than the number of variables implies. The BIC equation is therefore adapted to use the effective degrees of freedom, d_{eff}, rather than the raw parameter count,

$$\mathrm{BIC} = n \ln\left(\frac{\sum w_i (y_i - \hat{y}_i)^2}{n}\right) + d_{eff} \log n. \tag{1}$$

and

$$d_{eff} = \sum \frac{d_i^2}{d_i^2 + \lambda}, \tag{2}$$

where d_i are singular values of the predictor matrix - tabulated input variables used to fit the model - which summarise how much natural variation exists along each independent direction of the data. As λ increases, the regularisation more strongly constrains coefficients towards zero and the effective degrees of freedom, and therefore model complexity, reduces. This table is created using Regression_Methodology.ipynb.

3 SUPPLEMENTARY TABLE 3

Supplementary Table 3 details a synthetic flat portfolio of assets and includes the following information:

- Latitude, Longitude - Location of an asset.
- osm_id - unique identifier for each location.
- Type - details whether an asset is a hospital or energy facility.
- Limit Flat - total limit of the asset if 100% loss is achieved.

Locations of these assets are taken from Byers et al. [5] and Healthsites.io [6].

REFERENCES

[1] National Research Institute for Earth Science and Disaster Resilience. K-net, kik-net. Dataset, 2019. URL https://doi.org/10.17598/NIED.0004.

[2] Albert Kottke, Kris Vanneste, and Stef Bot. arkottke/pyrotd: v0.6.1, 2023. URL https://doi.org/10.5281/zenodo.8101955.

[3] RR-Inyo. shindo: Calculates JMA (Japan Meteorological Agency) seismic intensity (shindo) scale from acceleration data recorded in NumPy array. https://github.com/RR-Inyo/shindo, 2021. URL https://github.com/RR-Inyo/shindo. Accessed: 2026-06-01.

[4] Andrew A Neath and Joseph E Cavanaugh. The bayesian information criterion: background, derivation, and applications. *Wiley Interdisciplinary Reviews: Computational Statistics*, 4(2):199–203, 2012.

[5] Logan Byers, Johannes Friedrich, Roman Hennig, Aaron Kressig, Xinyue Li, Laura Malaguzzi Valeri, and Colin McCormick. A global database of power plants. Technical note, World Resources Institute, 2018. URL https://www.wri.org/research/global-database-power-plants.

[6] Healthsites.io. The global healthsites mapping project. https://healthsites.io/, 2026. Open healthcare facility dataset and API. Accessed: 2026-05-29.